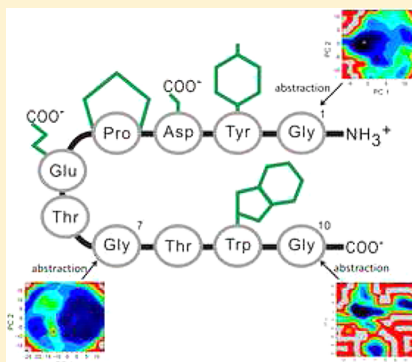


Site Specificity on OH α -H Abstraction Reaction for a Zwitterionic β -Hairpin Peptide in Aqueous Solution: A Theoretical Investigation

Ren-Jie Lin,[†] Soonmin Jang,[‡] Hyunsik Kim,[‡] Chen-Chang Wu,[†] and Feng-Yin Li^{*,†}[†]Department of Chemistry, National Chung Hsing University, Taichung, Taiwan 402, Republic of China[‡]Department of Chemistry, Sejong University, Seoul 143-747, Korea

S Supporting Information

ABSTRACT: Protein backbone oxidation was investigated by studying the α -H abstraction reaction in a β -hairpin peptide, called Chignolin (PDB ID 1UAO), with density functional theory calculation at B3LYP/6-31G(d,p) without any constraint. In order to stabilize the zwitterionic form of Chignolin with the salt bridges, the effects of aqueous solution were implemented by using microsolvation combined with a conductor-like polarizable continuum model (CPCM). Comparison between three glycine residues located at three different sites in Chignolin was used to examine the possible site specificity of this backbone oxidation. To construct the reaction profile of these α -H abstraction reactions, the pre- and postreactive complexes along with their associated transition states were located and verified with the intrinsic reaction coordinate (IRC) method. The bond dissociation energy and reaction rates of these OH α -H abstraction reactions were calculated with transition state theory. The differences in this abstraction reaction between the neutral and zwitterionic forms of Chignolin were also compared. A molecular dynamics simulation was implemented to study the explicit solvation effect on the abstracted Chignolin structure. The range of the simulation time scale covers from femtoseconds to microseconds, i.e., from onset of the abstraction to the abstracted products reaching thermal equilibrium. Our results show that there are three kinds of site-specificity in this abstraction reaction. The reactivity and stability of the abstraction products and their abstraction modes are all dependent on the location where OH attacks. Furthermore, the free energy landscapes of these abstraction products are distinctively different. This may imply that the pathological disorders or diseases caused by this type of radicals are also dependent on the abstraction location.



INTRODUCTION

Due to its relevance to various degenerative diseases related to pathological disorders and aging, radical-mediated protein oxidation attracts ever-increasing attention.^{1–5} These oxidations are believed to be initiated by reactive oxygen species (ROS), such as the superoxide radical, hydrogen peroxide, and the hydroxyl radical. Their oxidation products are also radicals and can attack other biomolecules to propagate damage in cells.^{4,5} During the past few decades, there have been various biomarkers identified to trace the oxidative pathways of related biomolecules;⁶ however, the whole picture of protein oxidation still remains unclear.

Of the protein and peptide radicals, the C_{α} -center radicals are prevalent in biological systems,⁷ because of the extensive stabilization through the captodative effect.^{8,9} This effect, proposed by Viehe et al.,¹⁰ is a combined action of a captor (electron-withdrawing) substituent and a dative (electron-donating) substituent on a single radical center, resulting in a stabilized carbon-center radical and unusually low C_{α} -H bond dissociation energies (BDEs).^{8,9,11–17} These C_{α} -center radicals are generated through α -H abstraction of an amino acid residue by ROS. It is generally believed that ROS attack a particular protein through a random process, i.e., either abstracting its α -H or attacking to the side chain of an amino acid residue.^{1–5}

However, it was shown that certain selectivity existed in this type of oxidation.^{18–20} For example, if the protein modifications were catalyzed by a transition metal, the metal and hydrogen peroxide would react at the metal-binding site to generate OH radicals, which in turn would attack the side chains of the nearby amino acid residues and the peptide bonds.^{18,19} Recently Lu et al. theoretically investigated the site specificity of the α -H abstraction by a hydroxyl radical among various secondary structural motifs.²⁰ They suggested that a prereactive complex is formed prior to the OH α -H abstraction, and the stability of the prereactive complex implies the chance of the abstraction at that particular site. Furthermore Cheng et al. proposed that the C_{α} -H BDE showed site specificity in a small peptide.²¹ If there are certain preferential sites in a given protein for ROS to attack, presumably one may predict where oxidation takes place and what those potential associated hazard products are.

Among many ROS found in biological systems, the OH radical is one of the dominant species and can be created intracellularly by a Fenton-type reaction, by Haber-Weiss

Received: September 6, 2012

Revised: December 12, 2012

Published: December 20, 2012

recombination, or by other radicals created from enzymatic reactions.²² Besides, the OH radical is the most reactive and biologically devastating because it is responsible for peptide bond cleavage.²³ Therefore the OH radical can serve as a typical reactant to study the oxidation reactions by ROS. The occurrence of α -H abstraction is determined by the competition between the α -H abstraction and other reactions to the side chains of the residues in a protein.^{24–26} Recently, the mechanism and kinetics of an OH radical reacting with various amino acids were investigated by Galano et al.^{24–28} to determine the branching ratio of α -H abstraction reactions taking place between the backbone and side chains. These branch ratios and associated transition states can be used to estimate the occurrence of an α -H abstraction site.

The investigations of α -H abstractions in proteins were done mostly through theoretical means mainly due to the short lifetime of C_{α} -center radicals. Because of the computational capacity, it is common practice in modern theoretical/computational studies to use model peptides or peptide fragments to reflect the local protein environment.^{8,9,11–15,24–29} For example, there were numerous studies on α -H abstraction reaction by using single amino acid residues^{24–29} and methyl-substituted glycine anion,²⁹ with or without structural restriction, to mimic secondary structures.^{8,9,11–15} Recently Lin et al.³⁰ used a molecular designed peptide, known as Chignolin (PDB ID 1UAO), to investigate the site specificity of the OH α -H abstraction. Composed of only 10 residues (GYDPETGTWG), Chignolin can fold into a unique structure with a cooperative thermal transition between its unfolded and folded states. So far, it is the smallest peptide that can form a stable β -hairpin in water.³¹ The electronic structure of Chignolin was studied by Fedorov et al.³² employing the fragment molecular orbital method.³³ In this study, we presented the results of oxidation damage to Chignolin in a more realistic model. In order to maintain the Chignolin native structure, i.e., zwitterionic form along with Asp3 and Glu5 in ionic form, the microsolvation coupled with conducting polarized continuum model (CPCM)^{34,35} was employed to simulate the effect of the aqueous solvation. The zwitterionic form of Chignolin, denoted as z-Chignolin, can be stabilized by microsolvation as reported by Fedorov et al.³² Furthermore, the effect of solvation for generating the $^{\text{a}}\text{C}$ -center radical in a glycine molecule was investigated by Wood et al.³⁶ through total free energy analysis. It had been reported in the literature^{37–41} that, if a gaseous condition was used during the structural optimization of an amino acid or peptide in zwitterionic form, the proton on the positively charged NH_3^+ group was transferred to the adjacent negatively charged COO^- group to form the neutral conformation without an energetic barrier. Therefore the neutral form of Chignolin, denoted as n-Chignolin, was solvated with only the CPCM model as reported in our previous work.³⁰ Since there are three glycines in Chignolin, which are located in the middle (Gly7), N-(Gly1), and C-terminal (Gly10), we investigated the α -H abstracted by OH radical from these three sites to study the difference in the reaction rate due to the site specificity. Although, compared to the α -H abstraction of the glycine residues, other types of OH radical reactions may be more favorable such as the attack at the simple alkyl C–H bonds of the proline and the addition reaction to the tryptophan residue in Chignolin since their reaction barriers are relatively lower than that of the α -H abstraction. However, in the current study

we only focused on the α -H abstraction of the glycine residues in Chignolin.

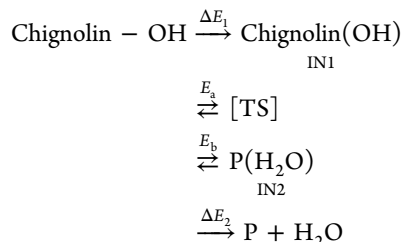
In addition to the quantum chemistry calculation, we also included the molecular dynamics (MD) simulation to explore the structural changes due to thermal relaxation. The abstracted structure obtained with density functional theory (DFT) optimization represents the conformation immediately after the abstraction takes place (within a few tens of femtoseconds) without interaction with the surrounding water molecules. While at the same time, the MD simulations are able to treat the interaction between the abstracted Chignolin and those surrounding water molecules explicitly and can provide trajectories with a time frame between nanoseconds and microseconds to locate the relaxed structures, presumably reaching thermal equilibrium. Therefore, combining the DFT optimization and MD simulation, we hope to provide the structural information regarding the relaxed conformations of the abstracted Chignolin in both a short and long time interval, respectively, after the abstraction takes place. In order to characterize the overall characteristics of thermodynamic behavior for the abstracted Chignolin, free energy landscape analysis was implemented by using principal component (PC) analysis. PC analysis, a standard mathematical tool used to detect correlations between the dominant features in a given data set, is a very useful method to examine the conformational sampling in an ensemble of configurations generated by either MD or Monte Carlo simulations, and is widely used.^{42–45} PC analysis is based on the diagonalization of the covariance matrix built from the positional fluctuations of the backbone atoms in MD trajectories and provides a means for sampling conformations. PC analysis also provides relatively robust parameters to describe the protein dynamics to generate free energy landscapes. It was shown that PC components are better suited than the conventional parameters such as radius of gyration (RG), root-mean-square deviation (RMSD), accessible surface area, number of hydrogen bonds, and native contact to characterize realistic free energy landscapes.⁴⁵

■ COMPUTATIONAL METHOD AND MODEL CONSTRUCTION

The initial structure of Chignolin was taken from the first one of the resultant 18 structures obtained by the NMR experiment.³¹ In order to construct the initial conformations with zwitterionic form and salt bridges, Chignolin was solvated with water molecules using the TIP4P model inside a cubic box of box length 37.94 Å, including two sodium ions to balance the negative charge. With current box size, the shortest distance between any of the Chignolin atoms and the box edge was 10 Å. The solvated Chignolin using an OPLS-AAL force field was subject to thermal equilibrium at 300 K for 50 ps MD simulation with NVT ensemble, i.e., isometric-isothermal ensemble with the number of molecules fixed, as implemented in the Gromacs MD package (ver. 4.5.5).⁴⁶ After thermal equilibrium, another 5 ns MD run under the same condition was performed, and the conformations along this run were saved at every 20 ps interval as candidates for the quantum chemistry calculations. The size of the fully solvated Chignolin with the calculation level used in this study is way beyond the reach of our computational capacity. Therefore, microsolvated Chignolin was used and generated by deleting all the water molecules in the saved structures from MD simulation, except those surrounding the charged residues, i.e., Gly1, Asp3, Glu5, and Gly10. In the current study, the OH abstraction reaction

from the z-Chignolin was performed with DFT as implemented in the Gaussian 03 (G03) package.⁴⁷ All species in the reaction path were fully optimized at the B3LYP/6-31G(d,p) level. The potential energy surface (PES) along the reaction pathway was characterized by performing intrinsic reaction coordinate (IRC) analysis.^{48–50} In order to estimate the zero point vibrational energy, harmonic vibrational frequency analysis at the same level was performed on the optimized structure without constraints. The CPCM combined with the United Atom for Hartree–Fock (UAHF) cavity, is an optimized combination method to obtain aqueous solvation free energies of the molecules in this study. Therefore, besides the microsolvation, the calculated aqueous solvation free energy of each species using CPCM-UAHF with the BHandHLYP/6-31G(d,p)//B3LYP/6-31G(d,p) level was added to the enthalpy at 0 K in gaseous conditions to mimic the reaction in an aqueous environment. We also used BHandHLYP/6-31G(d,p) to perform the similar structural optimization on the unreactive Chignolin to compare with the results obtained with B3LYP/6-31(d,p). The RMSD between the optimized structures obtained these two methods is 0.10 Å for all of the heavy atoms. This indicates that both methods generate almost the same optimized structure of the unreacted Chignolin. However, we were only able to locate the transition states of the middle abstraction reaction with the BHandHLYP/6-31G(d,p) level with RMSD against that obtained with B3LYP/6-31(d,p) being 0.19 Å for all of the heavy atoms. As to the other two abstraction reactions, we did not locate their transition states due to the long oscillation and not reaching the convergence criteria during the optimization processes. From the above structural comparison, we found there is only a small structural difference between the optimized structures obtained with BHandHLYP/6-31G(d,p) and B3LYP/6-31(d,p). Therefore we used B3LYP/6-31(d,p) for structural optimization and used the results of BHandHLYP/6-31G(d,p) with single point calculation throughout this study.

Because a glycine molecule has two α -H atoms, it is reasonable to assume that the α -H abstraction takes place on the α -H pointing outward from the peptide surface. The mechanism of OH α -H abstraction involved three steps as shown in the following scheme:



The reaction starts with the OH radical approaching Chignolin to form a hydrogen-bonding complex, which is the so-called prereactive complex (IN1). The existence of the prereactive complexes is required because the relative energy of the reactants before forming the prereactive complexes is higher than the transition states in some reaction paths. Then the α -H abstraction takes place at the transition state (TS), and the postreactive complex (IN2) is generated with the newly generated H₂O forming hydrogen bonds with the final product, the $^{\alpha}\text{C}$ -center radical. The forward reaction energy barrier (E_a) is an energy difference between TS and IN1, and so is the backward reaction energy barrier (E_b) between TS and IN2. The relative energy (ΔE_1) between the reactants and IN1 is an

important index for the stability of the prereactive complexes. Similarly, ΔE_2 is the relative energy between the final products and IN2, mostly due to the H-bonds between the C_{α} -center radical and newly formed water. To facilitate the study, we labeled the molecules investigated in this study by beginning with the prefix of the reaction species, such as IN1-, IN2-, TS-, and P- to represent the corresponding prereactive complex, postreactive complex, transition state, and C_{α} -center radical product, respectively, and then ending with the symbol of the corresponding site, such as m for Gly7, N for Gly1, and C for Gly10, respectively. We also added the prefix “z” for zwitterionic form and “n” for neutral form of Chignolin. For example, z-TS-N represents the transition state with the N-terminal α -H abstraction in zwitterionic form.

Investigating the site specificity of this abstraction reaction, i.e., the location of C_{α} -center radical in the α -H abstraction product, obviously depends on three factors: the availability of the to-be-abstacted α -H to the OH radical, the feasibility of the α -H abstraction, and the stability of the C_{α} -center radical. Therefore, three types of calculations were performed: searching the prereactive complex to estimate the availability of the to-be-abstacted α -H to the OH radical, and calculating the reaction rate constant and the C_{α} -H BDE for the feasibility of the α -H abstraction and the stability of the C_{α} -center radical product, respectively. The C_{α} -H BDEs, D^{α}_{CH} , for this hairpin, βH , defined as the heat of reaction (eq 1), was used to estimate the stability of the C_{α} -center radicals obtained from different abstraction sites. Instead of calculating $D^{\alpha}_{\text{CH}}(\beta\text{H})$ directly, it was derived from the heat formed from the isodesmic reaction⁵¹ (eq 2) to reduce the residual error associated with incomplete basis set and incomplete correction for electronic correlation, using glycine ($D^{\alpha}_{\text{CH}} = 349.8 \text{ kJ mol}^{-1}$)⁵² as a reference molecule, AH.



One can calculate $D^{\alpha}_{\text{CH}}(\beta\text{H})$ from Reaction 2:

$$D^{\alpha}_{\text{CH}}(\beta\text{H}) = D^{\alpha}_{\text{CH}}(\text{AH}) - \Delta H_{\text{iso}}^0 \quad (3)$$

where ΔH_{iso}^0 was calculated from the four species in eq 2.

As to the kinetic aspect, the rate constant without the tunneling effect at 298.15 K can be obtained by the following equation:⁵³

$$k_{\text{TST}} = \frac{k_{\text{B}}T}{h} \times \frac{Q_{\text{TS}}}{Q_{\text{IN1}}} e^{-(E_{\text{TS}} - T_{\text{IN1}})/k_{\text{B}}T} \quad (4)$$

where k_{B} and h are Boltzmann's and Plank's constants, and Q_{TS} and Q_{IN1} are the partition functions for transition state and prereactive complexes, respectively. Because we did not obtain the optimized structures at BHandHLYP levels, we used the partition functions from the results of the B3LYP level, obtained from G03 output directly, instead. In order to estimate the possible errors introduced by this replacement, we calculated the OH α -H abstraction of glycine at both B3LYP and BHandHLYP levels. The ratio of Q_{TS} and Q_{IN1} for the B3LYP level is 51.89 and that for the BHandHLYP level is 59.14. The main difference is contributed from the vibration term, and the details are provided in Table S1 of the Supporting Information. Since the difference of this ratio between these two levels is not large, the error introduced by this replacement should be limited. As to the influence of the conformational

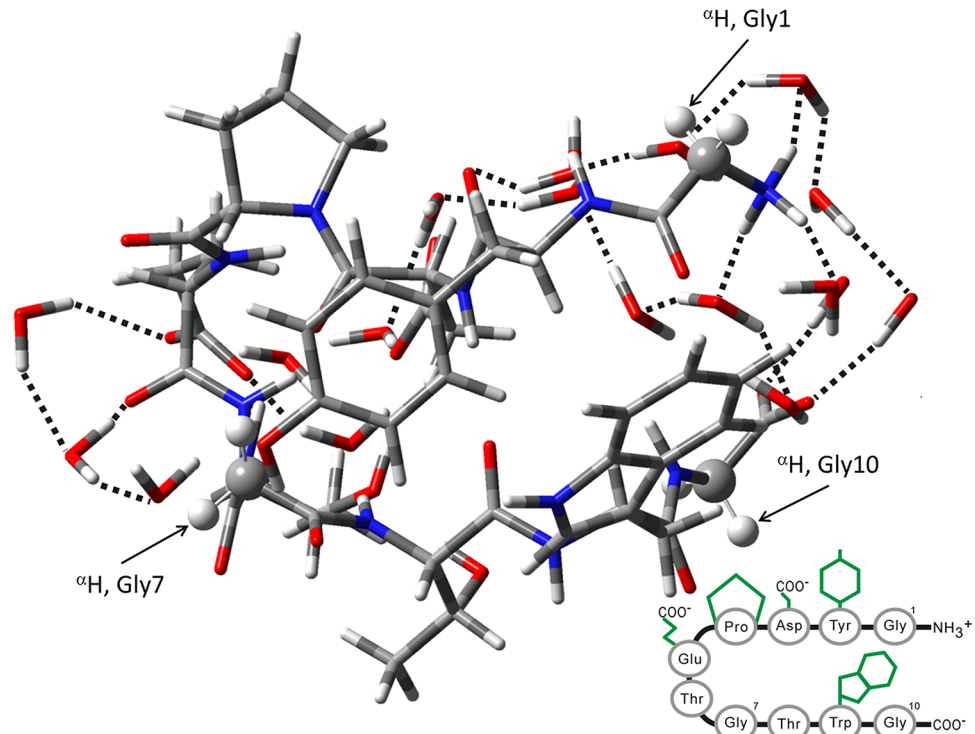


Figure 1. The optimized structure of z-Chignolin before the abstraction with the abstracted α -H atoms labeled as $^{\alpha}\text{H}$ and indicated by arrows and hydrogen bonds shown as dashed lines. The inset is a schematic plot for z-Chignolin.

flexibility in the prereactive complexes, transition states and postreactive complexes on the partition functions in the rate constant calculations, we performed cluster analysis,⁵⁴ provided in Gromacs, on the trajectories obtained from the MD simulations. The cluster analysis was done by sorting the sample conformations from MD simulations according to the RMSD value using the Chignolin NMR structure as the reference. The tunneling correction, κ , that due to the Wigner approach,^{55–57} is also applied

$$\kappa \approx 1 + \frac{1}{24} \left(\frac{\hbar \nu^{\ddagger}}{k_B T} \right)^2$$

where ν^{\ddagger} is the magnitude of the imaginary frequency of motion along the reaction coordinate at the transition state. The rate constants including tunneling correction are listed in Table 3. However, the Wigner approach is known to produce low quality values of κ , which are frequently underestimated to a large extent. For comparison, we also calculated the zero curvature tunneling correction developed by Skodje and Truhlar⁵⁸ to evaluate the possible errors. The results indicated that, only in the N-terminal abstraction of z-Chignolin does the κ value calculated by these two methods show large discrepancy: 13.76 for the method developed by Skodje and Truhlar, but 2.41 for the Wigner approach. The details of the comparison between these two methods for the abstraction reaction considered in this study are included in the Supporting Information. We also provided other information in the Supporting Information, including the Cartesian coordinates and vibration frequencies of all the chemical species in this study.

In order to explore the structural diversity due to the interaction with the surrounding water molecules, we performed a replica exchange molecular dynamics (REMD)

simulation^{55,56} to search the stable energy structures with explicit solvent solvation. The REMD simulation used in this study was implemented in a similar setting as those used in constructing the microsolvated z-Chignolin structure except for the force field involving the atoms associated with the radical. For those atoms, we adopted the same parameters used by Wood et al.,³⁶ which essentially came from the antechamber⁵⁹ module of the AMBER 10. The initial system was prepared with Amber10/Ambertools and the necessary parameters were converted to the Gromacs⁴⁶ format for MD simulation in Gromacs. The partial charges were obtained by restrained fitting to the electrostatic potentials (RESP)⁶⁰ derived from the BHandHLYP/6-31G(d,p)//B3LYP/6-31G(d) calculations mentioned above. As for REMD simulation, we used 37 different replicas, and the initial structure for each replica was prepared in several steps. First, the abstracted Chignolin after structural optimization with G03 was solvated in a periodic cubic box of TIP4P water molecules, similar to that used in constructing the z-Chignolin. In order to remove the unwanted interaction, the solvated Chignolin radical was subject to energy minimization followed by 100 ps NVT MD simulation at 300 K with the structure of the Chignolin radical fixed, allowing more wetting of the radical. After that, the resulting structure was subject to NPT MD simulation, i.e., simulation using isothermal-isobaric ensemble with the number of molecules fixed, for 1 ns at 300 K and 1 atm. Another NVT MD simulation was carried out for 3.7 ns at 400 K starting from the structure obtained above, and the conformations were saved at every 0.1 ns interval. The resulting 37 different structures were allocated to 37 different replicas as the initial structure for REMD simulation. This ensured the structural decorrelation between each replica, enabling more efficient sampling. The REMD temperature range was 300–504 K, and the replica exchange acceptance ratio was about 15% throughout the

REMD simulation. The REMD simulation time step was 2 fs with bond length constraint involving a hydrogen atom using the SHAKE method,⁵⁹ which solves the constraint equations determining the bond lengths using Lagrange multipliers added to the physical potential energy function governing the motion of the system. For temperature control, we used a modified Berendsen thermostat with a coupling constant of 0.1 ps as implemented in the Gromacs MD package. The long-range electrostatic force was calculated with particle mesh Ewald (PME) as implemented in Gromacs using the default values. The trajectory was saved at every 0.5 ps for further analysis. The total REMD time was 30 ns for each replica and 30 ns of trajectory; we discarded the initial 10 ns run in the final free energy landscape construction to ensure the convergence of the simulation.

As to the free energy landscape construction, the first and second principal components (PC1 and PC2) of the radical z-Chignolin were generated by diagonalizing the covariance matrix built from the positional fluctuations of the backbone atoms in MD trajectories, providing the dominant structural changes during the simulation. The free energy was calculated as $-RT \ln(P/P_0)$, where R is the gas constant, T is the temperature, P is the probability of finding the conformation at the given coordinate (PC1 and PC2), and P_0 is the normalized probability.⁴⁵ Also, we used the RMSD and RG as variables in free energy landscape analysis. As for the RMSD calculation, we used backbone atoms with the first PDB structure as reference.

RESULTS AND DISCUSSION

Construction of Microsolvated Zwitterionic Chignolin Structure. To construct the microsolvated Chignolin structures, we excluded all the water molecules beyond 5 Å from any atoms in each of the 250 candidate Chignolin structures obtained from MD simulation. We further deleted those water molecules that did not form a hydrogen bond with the water molecules that directly linked with a hydrogen bond to any one of the four charged sites, such as the carboxyl oxygen atoms in Asp3, Glu5, or Gly10 and the three amino hydrogen atoms in Gly1. Among these microsolvated Chignolin, 10 structures were chosen to perform structural optimization with the G03 package without any constraints because their numbers of solvated water molecules were under 20 since the system size with solvated water molecules over 20 was beyond the reach of our computational capacity. On the basis of the system size and structural stability, the optimized z-Chignolin solvated with 17 water molecules was selected, as shown in Figure 1. Table 1 showed the RMSD values of the n- and z-Chignolin against the original NMR structure for the heavy atom only and along with the other related Chignolin species. The results regarding n-Chignolin were taken from our previous study.³⁰ Although z-Chignolin was solvated in both microsolvation and bulk solvation, its structure was not much different from that of n-Chignolin, which was only in bulk solvation with RMSD against the original NMR structure just over 1 Å for all the heavy atoms. This indicated that the overall structure is not very sensitive to the charge difference of Gly1, Asp3, Glu5, and Gly10, i.e., the four charged sites. As to the hydrogen-bond network, z-Chignolin has only seven hydrogen bonds compared to the eight hydrogen bonds found in n-Chignolin, as shown in Table 2. The Asp3 acts as the key stabilization in the turn region of the hairpin by hydrogen bonding between Glu5, Thr6, Gly7, and Thr8 in n-Chignolin, but there is no hydrogen bonding between Asp3 and Glu5 in z-

Table 1. The RMSD of All the Related Species Calculated in This Study for All Heavy Atoms with the Unit as Å^a

	ref. geometry	1UAO	z-Chignolin	n-Chignolin
	Chignolin	1.052 (1.016) ^b		
N	IN1	1.065 (1.083)	0.057	0.285
	TS	1.065 (1.083)	0.170	0.394
	IN2	1.084 (0.947)	0.168	0.267
	P	1.037 (1.013)	0.147	0.123
	P-A ^c	3.005	3.117	
m	IN1	1.059 (0.991)	0.072	0.076
	TS	1.069 (0.986)	0.056	0.111
	IN2	1.104 (0.989)	0.250	0.263
	P	1.070 (1.016)	0.103	0.250
	P-A ^c	3.066	3.164	
C	IN1	1.064 (0.987)	0.055	0.320
	TS	1.076 (1.176)	0.163	0.425
	IN2	1.159 (1.056)	0.446	0.404
	P	1.149 (0.959)	0.443	0.315
	P-A ^c	4.329	4.710	

^aThe first column is the values of the z-Chignolin related species with respect to 1UAO (from PDB), while those of the n-Chignolin related species are in parentheses. The second and third columns are the RMSD of the z- and n-Chignolin related species with respect to their initial unreacted structures, respectively. ^bThe n-Chignolin structure was from Lin et al.³⁰ ^cThe structures of P-A (z-N, z-m, and z-C) were from the REMD simulation.

Chignolin. Furthermore, the hydrogen-bonding pattern of z-Chignolin is slightly different from that found in n-Chignolin, mostly on the four charged sites and the terminal regions. Before entering next section, there is one thing regarding the microsolvation treatment. In this study, the waters of microsolvation were treated as if they were structural waters in a crystalline protein. However, those waters belong to part of the first solvation shell and should be mobile and displaceable. According to the estimate by Dunitz,⁶¹ the range of the entropy gained for transferring one water molecule from a protein to bulk solvent was 0–7 cal mol⁻¹ K⁻¹, corresponding to the free energy ranging as 0–2 kcal mol⁻¹ at 300 K. Therefore we could assume that the gain of solvation entropy was no more than 119 cal mol⁻¹ K⁻¹ for the prereactive complex and transition state, if the rigid microsolvation assumption for the 17 microsolvation water molecules was removed. However, this correction for postreactive complex requires some extra care since there is one more water molecule generated after the OH radical abstracts one α -H from z-Chignolin. The number of water molecules microsolvating around z-Chignolin is 18, and therefore the gain of solvent entropy should be no more than 126 cal mol⁻¹ K⁻¹.

Reaction Profile. Figure 2 shows the reaction profiles of the OH α -H abstraction in the z- and n-Chignolin. The detailed energetic information along the reaction pathway and the rate constants at the BHandHLYP/6-31G(d,p) level with single point calculation are shown in Table 3. In order to include the entropy and temperature effects on the rate constants, we have to use the results calculated at the B3LYP/6-31G(d,p) level by using their frequency information. The rate constants of these three abstraction reactions at 298.15 K are 1.40×10^8 , 4.29×10^9 , and 1.79×10^9 M⁻¹ s⁻¹ for N-terminal, middle, and C-terminal abstraction, respectively. Obviously the rate constants obtained at the B3LYP level are much higher than those obtained at the BHandHLYP level. Our results indicated that this abstraction behaved differently toward these three sites.

Table 2. The Hydrogen Bonding of Chignolin and Its Associated Chemical Species in This Study

	N-form	IN1	IN2	product		Z-form	IN1	IN2	product
1	Gly1(C=O)...(H-N)Gly10	1.912	N	1.808	1.854	1	Asp3(C=O)...(H-N)Gly7	2.090	N
			m	1.907	1.898				m
			C	1.861	1.847				C
2	Asp3(C=O)...(H-N)Gly7	2.009	N	2.013	2.009	2	Asp3(C=O)...(H-N)Thr6	2.053	N
			m	2.046	-				m
			C	1.996	2.006				C
3	Asp3(C=O)...(H-N)Glu5	1.962	N	1.968	1.966	3	Asp3(C=O)...(H-O)Thr6	1.750	N
			m	2.027	2.023				m
			C	2.058	1.964				C
4	Asp3(C=O)...(H-N)Thr6	2.059	N	-	2.067	4	Thr6(H-O)...(H-N)Thr8	2.163	N
			m	-	2.029				m
			C	1.961	2.073				C
5	Glu5(C=O)...(O-H)Asp3	1.850	N	1.857	1.856	5	Thr6(H-O)...(H-O)Thr8	1.807	N
			m	1.853	1.854				m
			C	1.856	1.853				C
6	Thr8(C=O)...(H-N)Asp3	1.928	N	1.901	1.924	6	Gly7(C=O)...(H-O)Tyr2	1.758	N
			m	1.913	1.919				m
			C	1.957	1.940				C
7	Thr8(C-O)...(H-O)Thr6	1.831	N	1.823	1.831	7	Trp8(C=O)...(H-N)Asp3	2.003	N
			m	1.837	1.849				m
			C	1.843	1.839				C
8	Trp9(C=O)...(H-O)Thr8	1.900	N	1.878	1.895				N
			m	1.909	1.925				m
			C	1.953	1.955				C

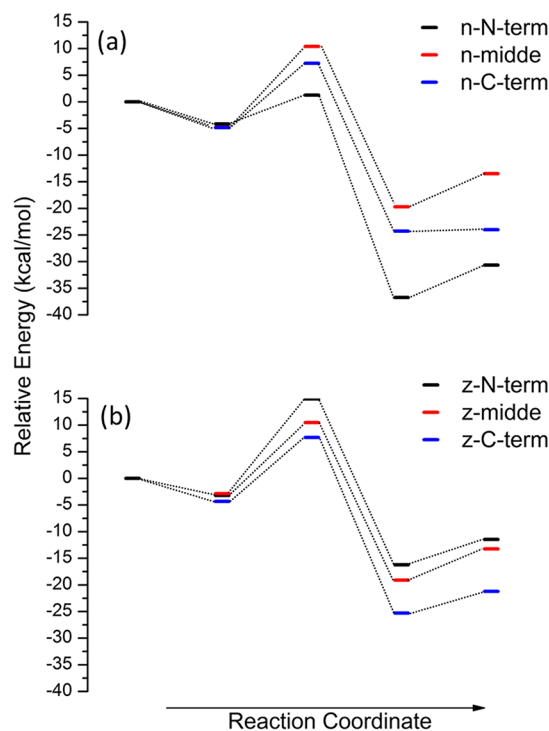


Figure 2. The energy profile of OH α -H abstraction at three different sites in both z- and n-Chignolin at the BH&HLYP/6-31G(d,p) level in aqueous solution.

Moreover, this site specificity also differed between these two forms of Chignolin. For example, the N-terminal abstraction in z-Chignolin has the highest activation energy with the lowest reaction rate constant, and its product is the least stable one with the least heat released. On the other hand, the reaction barrier of the C-terminal abstraction in z-Chignolin is the

lowest one and its abstraction product is the most stable one among the three related products. As to n-Chignolin, the N-terminal abstraction is the favorite channel both kinetically and thermodynamically with the lowest energy barrier and relative energy. The middle abstraction is the most difficult reaction channel for n-Chignolin with the lowest rate constant. Interestingly, the reaction barrier of the N-terminal abstraction in z-Chignolin is almost 3 times as large as that found in n-Chignolin, and therefore the difference in the reaction rate constant is enormous, reaching 10^8 fold. However the C-terminal abstraction in both forms of Chignolin behaves quite similarly and so does the middle abstraction. To investigate the origin of this site specificity, we analyzed the structural changes and their related electronic properties of the chemical species in each step of the reaction profile.

Change in Molecular Structure Due to Abstraction. As shown in Table 1 and Figure 3, our results from G03 calculation showed very limited structural changes, even though the α -C of the oxidized glycine residue switched from sp^3 - to sp^2 -bonding after abstraction, due to the intramolecular hydrogen bonding interaction, but this is because those conformations were calculated at 0 K, i.e., without thermal fluctuation, and should be considered as the conformations right after the abstraction without thermal equilibrium. Under this consideration, the hydrogen bonding network of the abstracted n-Chignolin remains almost the same as that of the corresponding reactant except for the interaction between Asp3 and Thr6 missing in the n-IN2-n and n-IN2-m. As to the abstracted z-Chignolins, the hydrogen bonding network experienced slightly larger change than that found in the abstracted n-Chignolins, especially the middle-abstracted one. However, this intramolecular hydrogen bonding interaction can not maintain the hairpin structure in those conformations after thermal relaxation. In order to demonstrate these structural changes, the abstracted z-Chignolin for each of the three

Table 3. The Energy Barrier, Enthalpy, and Reaction Constant of the α -H Abstraction of Glycine at Three Different Sites for z- and n-Chignolin as Calculated at the BHandHLYP/6-31G(d,p) Level with Single Point Calculation

species	ΔE_1 (kcal/mol)	ΔE_2 (kcal/mol)	E_a (kcal/mol)	E_b (kcal/mol)	ΔH (kcal/mol)	k_{TST} ($M^{-1} s^{-1}$)	k^b ($M^{-1} s^{-1}$)
z-N-term	-11.72 (-3.20) ^a	8.56 (4.79)	16.46 (18.13)	25.06 (31.17)	-8.60 (-13.04)	1.40 (8.32×10^{-2})	3.37 (2.01×10^{-1})
n-N-term	-13.70 (-4.15)	14.22 (6.09)	6.68 (5.40)	38.92 (38.00)	-32.24 (-32.60)	3.89×10^8 (3.34×10^8)	3.91×10^8 (3.36×10^8)
z-middle	-8.70 (-2.86)	13.13 (5.89)	13.09 (13.36)	31.67 (29.62)	-18.58 (-16.27)	2.70×10^2 (1.72×10^2)	3.56×10^2 (2.28×10^2)
n-middle	-10.74 (-4.78)	10.60 (6.22)	14.66 (15.18)	28.75 (30.11)	-14.08 (-14.94)	2.86×10 (1.21×10)	4.98×10 (2.09×10)
z-C-term	-9.87 (-4.31)	9.11 (4.07)	8.94 (12.00)	30.01 (32.99)	-21.07 (-20.99)	2.95×10^5 (1.70×10^3)	3.30×10^5 (1.90×10^3)
n-C-term	-13.43 (-4.84)	7.38 (0.27)	11.82 (12.08)	33.16 (31.54)	-21.34 (-19.46)	2.87×10^3 (1.85×10^3)	2.99×10^3 (1.92×10^3)

^aValues in parentheses include the CPCM solvation. ^b $k = \kappa \times k_{\text{TST}}$, where κ is the tunneling correction as described in the text.

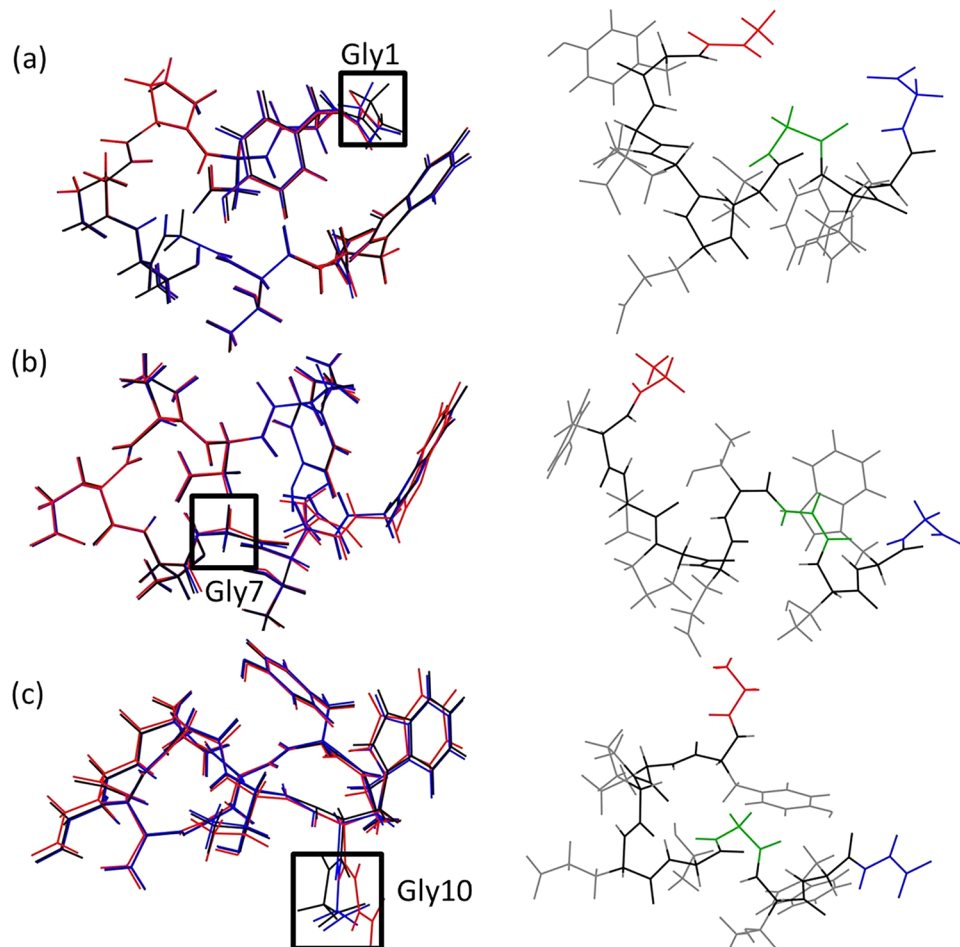


Figure 3. The comparison between the three abstracted z-Chignolin structures obtained from G03 calculations and REMD simulations, where (a), (b), and (c) are the abstractions that happened at the N-terminal, middle, and C-terminal glycine of z-Chignolin, respectively; the left column is the results from G03 calculations, and the right column is those from REMD simulations.

different abstraction reactions with the lowest energy was chosen from the conformations obtained in the REMD simulation. The RMSD values of the abstracted products for N-terminal, middle, and C-terminal abstraction against 1UAO NMR structure obtained with REMD calculation are 8.222, 8.864, and 10.589 Å, respectively. The large structural changes were also observed in the abstraction of n-Chignolin.³⁰ As shown in Figure 3 and Table 4, the hairpin structure of

Table 4. The Geometric Characteristics of the z-Chignolin and Its Related Abstracted Products

	G1-P4	P4-G7	G7-G10	G1-G10	P4-G10	G1-G7
z-Chignolin	9.32	5.33	9.13	7.32	10.45	10.68
N-term	6.20	4.69	5.45	7.14	10.12	4.08
mid	7.93	6.44	5.27	13.66	11.46	9.16
C-term	8.71	4.84	7.02	11.82	11.82	8.49

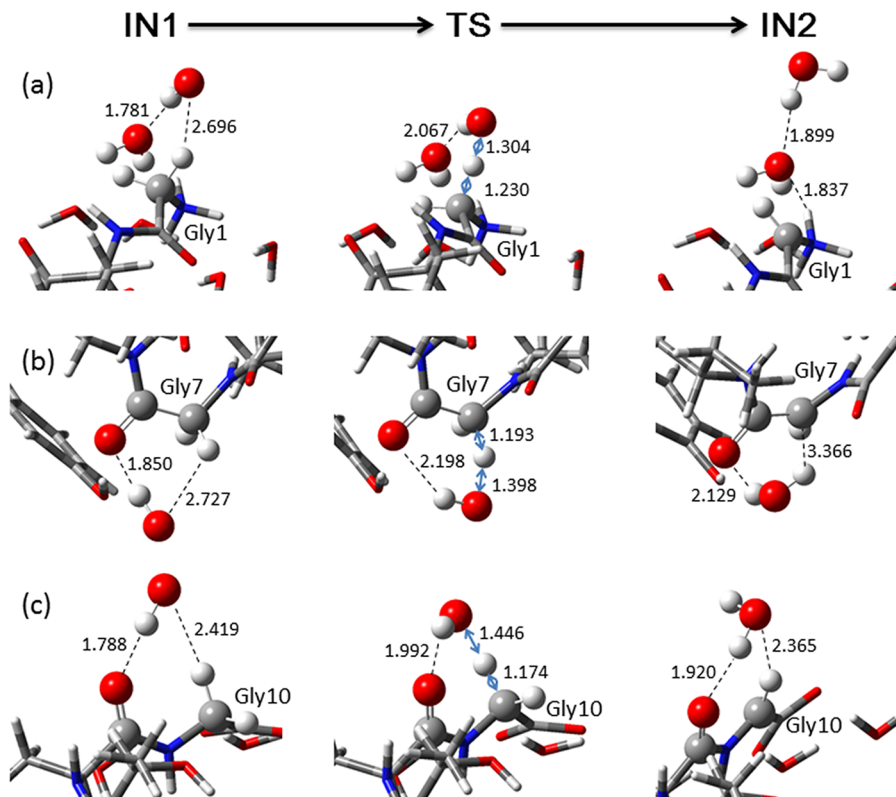


Figure 4. The important geometric parameters along the reaction pathway for three abstraction sites discussed in this study. (a), (b), and (c) are the abstractions that happened at the N-terminal, middle, and C-terminal glycine of z-Chignolin, respectively, with the prereactive complex in the first column, and the transition state in the middle, and followed by the postreactive complex. The red, blue, white, and gray balls represent oxygen, nitrogen, hydrogen, and carbon atoms, respectively.

Chignolin was severely twisted by bending the two β -strands, i.e., the shrunken distances between the α -C carbons of Gly1 and Pro4 and between those of Gly7 and Gly10. Even though the two β -strands were separated widely as shown in the distance between the α -C carbons of Gly1 and Gly10 in the middle and C-terminal abstraction, the shape of the turn region in the hairpin remained or became even tighter as seen in the distance between the α -C carbons of Gly7 and Pro4. It is because there are several hydrogen bonds in the turn region of these three abstracted z-Chignolin obtained by REMD simulation. This implies that, with enough hydrogen bonds, the secondary structure can sustain the large structural changes caused by single OH abstraction on the α -H. In the following, we analyzed the effects influencing these OH abstraction reactions, step by step along the reaction pathway, to explain the above structural changes.

Stability of the Prereactive Complex in Different Abstraction Sites. The lifetime of the prereactive complexes can be measured by their stability, and therefore it is a useful index to determine the probability of a particular α -H to undergo the OH abstraction reaction. As shown in Table 2, the relative energies of the prereactive complexes in these three abstraction sites are different. For both the z- and n-Chignolins, the IN1-C is the more stable than IN1-N and IN1-m, when bulk solvation is included. The z-IN1-C and n-IN1-C have similar stabilities with respect to the isolated reactants, i.e., OH radical and z-Chignolin separated infinitely. The different stabilities of the prereactive complexes imply the location and orientation, where and how the OH radical abstraction reaction may take place. Obviously it is the hydrogen bonds that

stabilize the prereactive complex and then determine the relative stability among the prereactive complexes. It is intrinsically different between z- and n-Chignolins to hydrogen bonding with the OH radical. For n-Chignolin, the OH radical has to form a hydrogen bond directly with the side chain or backbone of the peptide since only bulk solvation is included. The main difficulty in searching the suitable prereactive complexes for n-Chignolin is that there are not many hydrogen acceptors around the abstracted site to stabilize the complexes. It is very sensitive toward the peptide conformation. As for z-Chignolin, things are quite different because microsolvation is considered. The approaching OH radical can either form hydrogen bonding with the peptide itself or with the surrounding water molecules. However, the main difficulty to find the suitable prereactive complexes of the microsolvated Chignolin is that there are too many conformations as possible candidates. It will take lengthy calculations to verify whether these candidates do lead to the abstraction. In order to facilitate the calculation, we used the OH α -H abstraction in a microsolvated glycine in our previous work³⁰ as a template to construct these prereactive complexes by placing the OH radical in the promising location. The results of the hydrogen bonding patterns found in prereactive complexes for n- and z-Chignolins are quite different. For example, in z-IN1-N the OH radical forms a hydrogen bond with a water molecule, and this water molecule also forms a hydrogen bond to the NH_3^+ terminal end, as shown in Figure 4. As to the n-IN1-N, the OH radical forms a hydrogen bond with the carbonyl oxygen of the Tyr2 residue. Interestingly, in both z-IN1-m and n-IN1-m, the OH radical forms a hydrogen bond with the abstracted residue.

However, the OH radical forms a hydrogen bond with the carbonyl oxygen in the backbone of the Trp9 residue for z-IN-C but for n-IN1-C it is the carboxyl oxygen in Gly10, which the radical forms a hydrogen bond with. Searching prereactive complexes is the most time-demanding and troublesome step in the calculations of these abstraction reactions. Although the energy difference between the prereactive complexes in these three abstraction sites is rather small, it is the critical step in the site specificity of this abstraction reaction since it determines the location and orientation of the OH radical attacking the α -H in a particular residue. It leads to the next step, i.e., how feasible the abstraction is after the prereactive complex forms.

Abstraction Mode and Energy Barrier in Transition State.

As shown in Table 3, the energy barrier varies between the three different abstraction sites of the zwitterionic and neutral forms. In n-Chignolin, the energy barrier of the N-terminal abstraction is the lowest among the three abstraction sites, but it is the highest one in z-Chignolin. The reason can be explained by the abstraction modes, which were described in our previous study.³⁰ There are three different abstraction modes as found in the abstraction reaction of n-Chignolin, i.e., the stretching mode with large imaginary frequency found in n-TS-m, the rotation-like mode with small imaginary frequency in n-TS-N, and the bending motion, a mixture of the stretching and rotation-like modes, with imaginary frequency being between the frequencies of the previous two modes, as found in the n-TS-C. The abstraction mode of z-TS-N is similar to that of the n-TS-m, mostly a stretching motion of the abstracted α -H between the corresponding α -C and OH radical, as shown in the middle column of Figure 4. The animation of these abstraction motions are provided in the Supporting Information. Interestingly the imaginary frequency of z-TS-N is 2 times more than that of z-TS-m and 3 times more than that of z-TS-C. It is because the abstraction modes in both z-TS-m and z-TS-C are bending modes, like that found in n-TS-C.

In order to investigate the change in the electronic structure of z-Chignolin during the abstraction for the three abstraction sites, we measured the spin density. Originally, all the spin density was on the OH radical, and spin density transferring to Chignolin took place when the transition state forms. As shown in Figure 5, there are 39.4, 35.2, and 25.1% spin densities transferred from OH radical to Chignolin in z-TS-N, z-TS-m, and z-TS-C, respectively. Significant spin transfer was found for all the three abstractions. However, compared to n-Chignolin, there are 4.9, 38.3, and 21.1% spin transfers from the radical for the n-TS-N, n-TS-m, and n-TS-C, respectively. It was found that the more the spin density of α -C in the transition state, the higher the energetic barrier of the α -H abstraction reaction. There is a distinctive difference in spin transfer for N-terminal abstraction between n- and z-Chignolins, but the spin transfer for the other two abstraction reactions is not much different between these two forms. The main reason for the small energetic barrier for the N-terminal abstraction and the subsequent stability of its product found in n-Chignolin is due to the captodative effect as described in our previous work.³⁰ Obviously the NH_3^+ terminal of z-Chignolin is the main reason for the high energetic barrier, large imaginary frequency of the abstraction mode, and low reaction rate constant in the N-terminal abstraction for z-Chignolin compared to its n-Chignolin counterpart. However, for the C-terminal abstraction, there is not much deviation between the neutral and zwitterionic forms. It is because the resonance

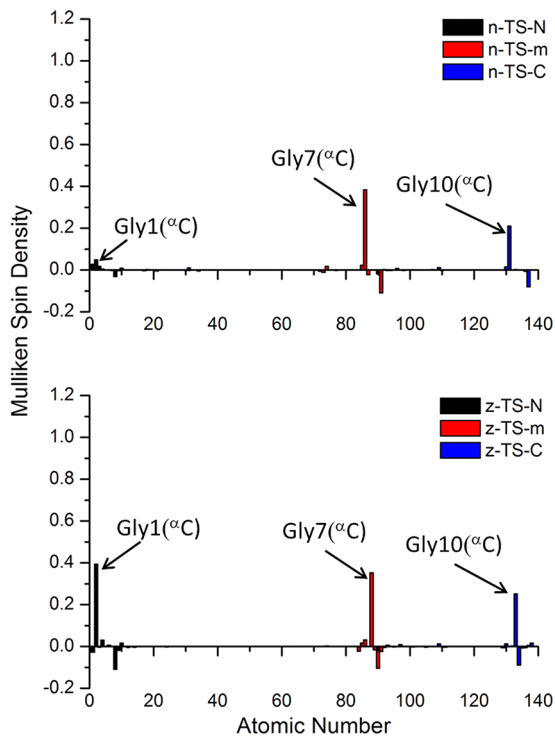


Figure 5. Mulliken atomic spin of transition states for the three abstraction sites, where the peaks with large intensity are labeled with the corresponding residue name and the specific atom in parentheses.

effect to stabilize the structure is mainly between the α -C and nitrogen atoms. Therefore the C-terminal abstraction in zwitterionic form has very limited stabilization from the resonance as that found in neutral form.

Before discussing the postreactive complex, it is worthwhile to note that our rate calculations were done without considering the influence of the conformational flexibility on the partition functions of the prereactive complex (Q_{IN1}) and transition state (Q_{TS}). However, it is rather difficult to perform structural sampling within G03 calculations, especially with the system size of this study. Nevertheless the effects due to the conformational variability, i.e., contribution of thermal equilibrium between Chignolin and surrounding water molecules to the partition functions of both Q_{IN1} and Q_{TS} , can be discussed with cluster analysis combining with the abstraction modes as described above. We estimated the backbone RMSD distribution from MD trajectories with the 1UAO NMR structure as a reference after discarding the initial 10 ns of simulation trajectory. According to this analysis (Figure 6) for the native Chignolin, around 80% of the sampled conformations were within RMSD 2.5 Å. It means the OH abstraction most likely takes place with the conformations similar to the 1UAO NMR structure. Therefore the effects of conformational variability on the partition function of the prereactive complex should mostly come from the side chain motion of the residues in Chignolin, mainly the torsion angle, but the conformational variability of their backbone was locked by the hydrogen bonding network. The geometries of the prereactive complexes can be characterized according to the way how the approaching OH radical is stabilized by hydrogen bonds with Chignolin. They could be roughly divided into two categories, i.e., direct and indirect stabilization through the interaction with the residues of Chignolin. For example, z-IN1-m belongs to the first category and z-IN1-N belongs to the second category,

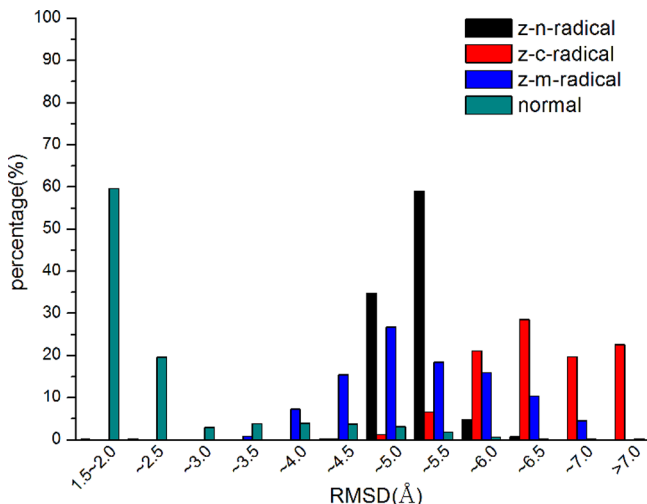


Figure 6. RMSD distribution of native z-Chignolin and its postreactive complexes for the three abstraction sites obtained from REMD simulations, where the backbone RMSD values were calculated using the IUAO NMR structure as the reference.

which are stabilized by interacting with the water molecules belonging to the first solvation shell. Therefore, the Q_{IN1} of the second category should also include the translational variation of those interacting water molecules in the prereactive complexes. As to transition states, we can use the abstraction mode to describe the influence of the conformational flexibility on Q_{TS} . In the stretching mode, the conformational variation between the transition state and its corresponding prereactive complex is mainly the abstracted α -H oscillating between the corresponding α -H and OH radical, and therefore requires small conformational variability correction. For the rotation-like mode, the transition state requires the rotation-like motion of the neighboring atoms along with the motion of the abstracted α -H, and therefore the conformational variation correction on Q_{TS} is the largest one among the three abstraction modes. As to the bending mode, the value of this conformational variation correction on Q_{TS} is between the above two modes.

Stability of the Postreactive Complex in Different Abstraction Sites. After the α -H abstraction is completed, the newly formed H_2O remains close to the oxidized Chignolin to form a postreactive complex through some hydrogen bonds, as shown in the third column of Figure 7. This newly formed H_2O will quickly lose this identity through rapid exchange with the surrounding water molecules. Therefore the lifetime of these postreactive complexes is rather short, and their properties should be almost the same as the associated oxidized Chignolin. Because the energy barriers of the reverse reaction are rather high, it is rather pointless to discuss the reverse reaction of the postreactive complexes. Therefore we focused on the effects influence on the stability of these postreactive complexes and the structural change for the subsequent thermal relaxation.

As shown in Figure 2, n-IN2-N has the lowest relative energy among the three postreactive complexes. This is mainly due to the captodative effect to stabilize the C_α -center radical formed after the α -H abstraction. The C_α -center radical in n-IN2-N also has a lower spin density than the C_α -center radical in the other two postreactive complexes as shown in Figure 7. This implies that the spin density of the C_α -center radical can delocalize to neighboring amino acids, and this delocalization stabilizes the whole structure. However, it is quite different for

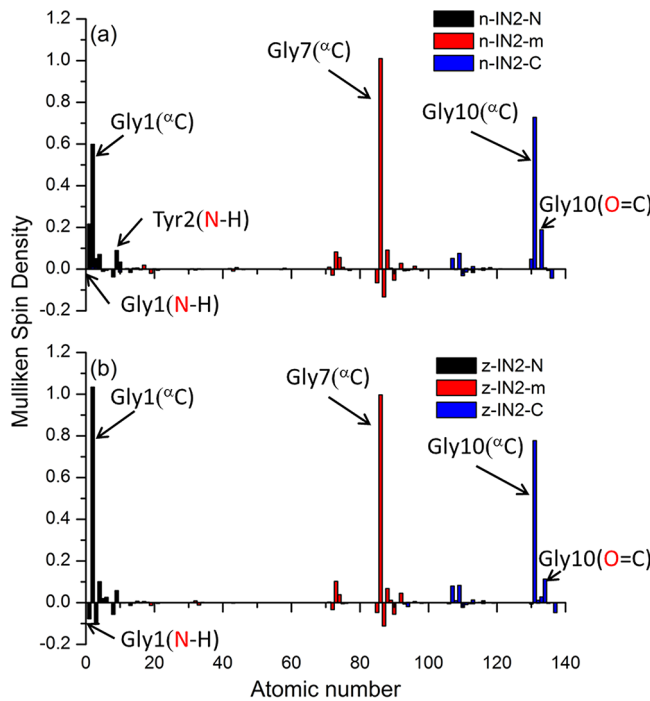


Figure 7. Mulliken atomic spin of the postreactive complexes for the three abstraction sites, where the peaks with large intensity are labeled with the corresponding residue name and the specific atom in parentheses (or the one indicated in red color if more than two atoms).

z-Chignolin since all three postreactive complexes share a similar pattern in the spin density distribution. It means that there is no captodative effect to stabilize the C_α -center radical of z-IN2-N, and the delocalization of spin density among the neighboring amino acids does not exist, due to the NH_3^+ group in the abstraction product of z-IN2-N. Similar phenomena are also observed in the C_α -H BDEs of the three abstracted products of Chignolin, which were calculated through isodesmic reactions using glycine as a reference. The reaction heats of the three isodesmic reactions with zero point energy correction related to z-P-N, z-P-m, and z-P-C were -17.23, -15.52, and -7.40 kcal/mol, respectively. However the reaction heats of the three isodesmic reactions of n-P-N, n-P-m, and n-P-C were -2.23, -15.34, and -11.35 kcal/mol, respectively. As shown in Table 5, the results indicate that there is a preferential α -H abstraction location in neutral IUAO. Because of the captodative effect to make this radical stabilized, the C_α -H BDE for the N-terminal glycine was lower than the other two glycines. However, the C_α -H BDE of z-P-N, z-P-m, and z-P-C are all larger than that of glycine, and there is no

Table 5. The Geometrical Parameters of Transition State of n- and z-Chignolin, along with Their Imaginary Frequencies and BDEs of the Abstraction

	${}^\alpha C - {}^\alpha H$	${}^\alpha H - O_{\text{radical}}$	${}^\alpha C - {}^\alpha H - O_{\text{radical}}$	imaginary freq.	BDE (kJ/mol)
z-TS-n	1.229	1.304	153.9	1209.3	403.0
z-TS-m	1.193	1.398	155.9	577.8	395.9
z-TS-c	1.173	1.446	158.3	349.8	361.9
n-TS-n	1.137	1.781	142.4	79.5	321.7
n-TS-m	1.224	1.330	154.8	875.3	395.1
n-TS-c	1.169	1.479	159.0	205.5	378.5

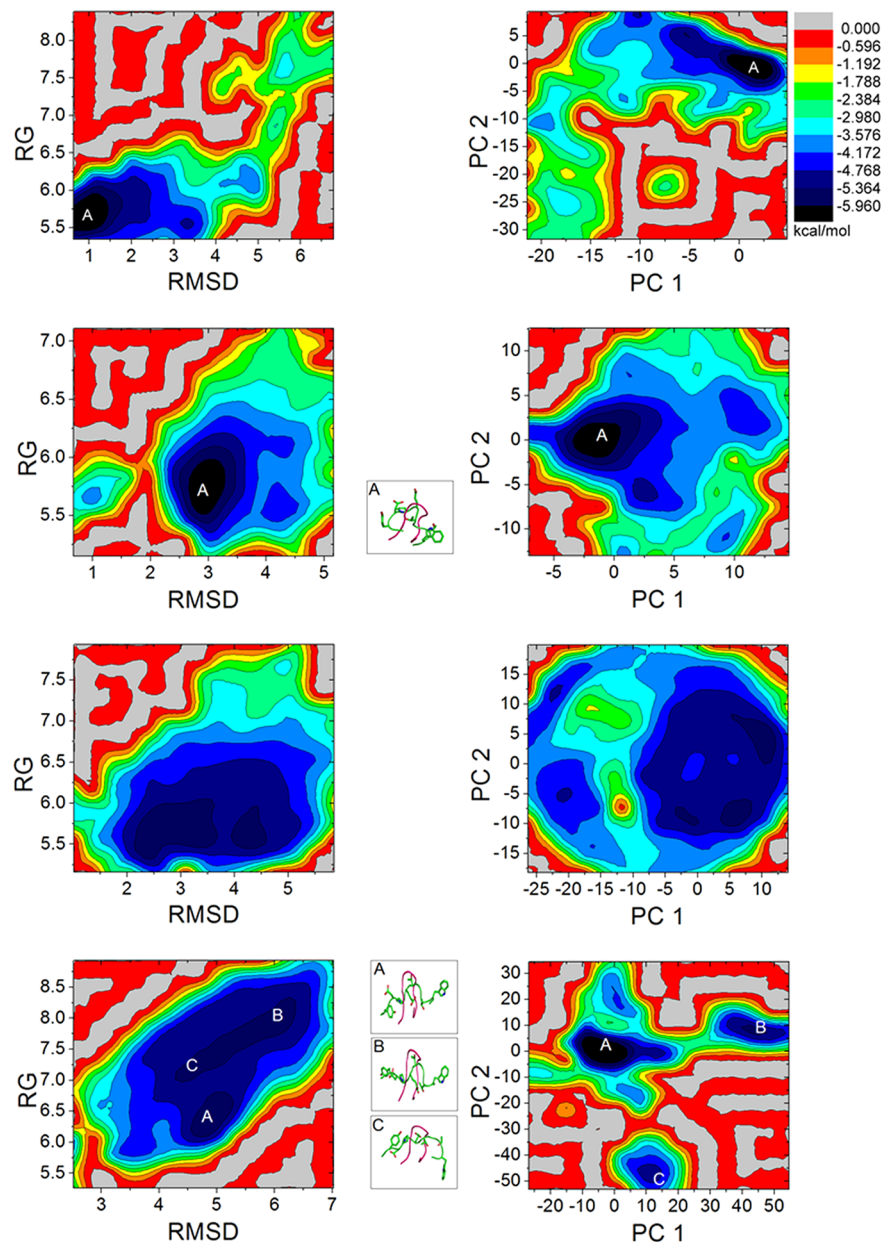


Figure 8. The free energy landscapes of the native and three abstracted z-Chignolin obtained from REMD simulations, where the plots from top to bottom are the native and abstraction happened at the N-terminal, middle, and C-terminal glycine of Chignolin, respectively; the plots in the left column are the free energy landscapes in (RMSD, Rg) space, and those in the right column are the free energy landscapes in PC space with the representative conformation in the middle for each defined basin shown in green and the native structure in pink. Note that the label A in the landscape plot represents the global free energy minimum basin for the particular chemical species.

captodative effect in z-P-N. These results explain why the heat released by the N-terminal abstraction reaction from z-Chignolin is substantially smaller than its neutral counterpart.

Our results obtained by G03 calculations showed very limited structural changes after abstraction, but this phenomenon is because those conformations were calculated at 0 K, i.e., without thermal fluctuation. It is important to know whether the intramolecular hydrogen bonding interaction of those abstracted conformations can hold together the hairpin structures under thermal equilibrium with surrounding solvent. For this reason, we applied REMD simulation to the abstracted Chignolin to demonstrate the structural stability through free energy landscape analysis. The eigenvalues of the first two PC components (PC1 and PC2) comprise about 65% of the total

fluctuations in the middle-abstracted Chignolin. Conventionally, RMSD and RG are commonly employed as the coordinate since these variables are physically more intuitive. For comparison, we also performed another REMD simulation for native Chignolin, and its free energy landscape was constructed. Figure 8 shows the free energy contour maps for the native and three abstracted Chignolins with respect to the PC1 and PC2 of the radicals, along with their counterparts in RMSD and RG. The contour line interval was set to $k_B T$ at room temperature, i.e., 0.596 kcal/mol, where k_B is Boltzmann's constant and T is absolute temperature. One can immediately notice that the normal Chignolin has well-defined single free energy basin in both PC spaces and (RMSD, RG) space, suggesting that unique structure, the hairpin in this case, exists

in the simulation. The free energy of N-terminal abstracted Chignolins has one relatively well-defined basin both in PC space and (RMSD, RG) space, but there are three for C-terminal abstracted Chignolin. This suggests that N-terminal abstracted Chignolin has a single distinctive structure like the native one, but the structural fluctuation is much larger than that of the native one. For C-terminal abstracted Chignolin, loosely speaking, there are three structures with large structural variations. We have selected representative structures corresponding to each free energy basin for both N- and C-terminal abstracted Chignolins and shown along with free energy plots. The representative structure is overlapped with native structure, which is shown in magenta. In fact, the representative structures have one-to-one correspondence, showing the free energy consistency both in PC space and (RMSD, RG) space. In other words, the results structurally show that the C-terminal abstracted Chignolin can be divided into three categories according to the native structure with their molecular size larger than the native one and undergoing larger structural fluctuation between these three basins, corresponding to the structural fluctuation in the two terminal regions. The results indicate that the two terminal regions undergo opening and closing with the turn region remaining relatively stable. Interestingly, energy basins for the middle-abstracted Chignolin both in PC spaces in (RMSD, RG) space indicate that it has a very broad energy basin without distinctive structures, unlike the C-terminal radical with three structures. The change of the molecular size for middle-abstracted Chignolin is confined within a certain range, but its conformation undergoes large changes. This indicates that the free energy differences between these basins are minimal and can be easily crossed with thermal energy at this temperature (300 K), i.e., at least in this case, the structure of this short peptide is not uniquely defined after the abstraction. Perhaps, the pathological disorders or disease in the presence of ROS may be closely related to these highly unstable structureless protein or peptide radicals. The results indicate that the structural diversity of the C-terminal radical is larger than the middle-abstracted radical and more like that found in the N-terminal radical with larger energetic barriers. The site specificity of this α -H abstraction reaction is also found in the final abstraction products, such as the differences in their free energy landscapes. The reasons for this site specificity are the following. The α -H abstraction causes the bonding type of the abstracted α C from sp^3 to sp^2 to undergo structural change to release this structural strain. However, the structures of the middle abstracted Chignolin, such as the one shown in Figure 3b, are the conformations with the interaction that can balance between the above structural strain and the resistance from the local hydrogen bonds, which is the main interaction to maintain the structural stability. At the same time, this changes the free energy landscape of Chignolin to lose the ability to maintain the well-defined β -hairpin structure. Meanwhile, the same bonding type change at terminals also induces some structural changes in smaller magnitude to the overall peptide structure since the above structural strain can be released to surrounding water molecules through terminal motions. It is not clear at this moment whether the current findings are general features of α -H abstracted peptides or proteins. Since the α -H abstracted Chignolin is highly reactive, there is a possibility that its lifetime is so short that it may not fully explore the whole free energy landscape to relax to its thermodynamic equilibrium state due to the reaction with other biomolecules, such as lipids or other proteins, *in vivo*.

CONCLUSION

We have successfully demonstrated the OH α -H abstraction of Chignolin with full ab initio calculation in aqueous environment by combining both microsolvation and bulk solvation. The range of the simulation time scale covers from femtoseconds to microseconds, i.e., from onset of the abstraction to the abstracted products presumably reaching thermal equilibrium. The structures of Chignolin and three α -H abstracted products along with their associated transition states were fully optimized at the B3LYP/6-31G(d,p) level. There exists site specificity between these three α -H abstraction reactions for z-Chignolin. However, it is not as prominent as those found in their neutral counterparts. In n-Chignolin, the energy barrier of the N-terminal abstraction is the lowest among the three abstraction sites, but it is the highest one in z-Chignolin. The main reason for the small energetic barrier for the N-terminal abstraction and the subsequent stability of its product found in n-Chignolin is the captodative effect, but this effect is not observed in z-Chignolin because of the NH₃⁺ terminal of z-Chignolin. Furthermore, REMD simulation along with the free energy landscape analysis was performed to investigate the structural change due to the abstraction with thermal relaxation. The results indicate that the middle-abstracted Chignolin has no well-defined structures and undergoes rapid conformational changes. However, the abstracted Chignolins in both termini possess a set of relatively well-defined structures with more structural diversity for C-terminal abstracted Chignolin.

ASSOCIATED CONTENT

S Supporting Information

The Cartesian coordinates and vibration frequencies of all the chemical species used in this study, and motion pictures of the abstraction modes. This material is available free of charge via the Internet at <http://pubs.acs.org>.

AUTHOR INFORMATION

Corresponding Author

*E-mail: feng64@nchu.edu.tw.

Notes

The authors declare no competing financial interest.

ACKNOWLEDGMENTS

The authors thank the National Science Council for financial support. The National Center for High-Performance Computing is acknowledged for providing computational resources.

REFERENCES

- (1) Stadtman, E. *Science* **1992**, 257, 1220–1224.
- (2) Stadtman, E. R. *Free Radical Biol. Med.* **2002**, 33, 597–604.
- (3) Stadtman, E. R.; Levine, R. L. *Amino Acids* **2003**, 25, 207–218.
- (4) Stadtman, E. R.; Van Remmen, H.; Richardson, A.; Wehr, N. B.; Levine, R. L. *Biochim. Biophys. Acta* **2005**, 1703, 135–140.
- (5) Stadtman, E. R. *Free Radical Res.* **2006**, 40, 1250–1258.
- (6) Uchida, T.; Unno, M.; Ishimori, K.; Morishima, I. *Biochemistry* **1997**, 36, 324–332.
- (7) Easton, C. J. *Chem. Rev.* **1997**, 97, 53–82.
- (8) Rauk, A.; Armstrong, D. A. *J. Am. Chem. Soc.* **2000**, 122, 4185–4192.
- (9) Rauk, A.; Yu, D.; Taylor, J.; Shustov, G. V.; Block, D. A.; Armstrong, D. A. *Biochemistry* **1999**, 38, 9089–9096.
- (10) Viehe, H. G.; Merényi, R.; Stella, L.; Janousek, Z. *Angew. Chem., Int. Ed. Engl.* **1979**, 18, 917–932.

- (11) Armstrong, D.; Yu, D.; Rauk, A. *Can. J. Chem.* **1996**, *74*, 1192–1199.
- (12) Rauk, A.; Yu, D.; Armstrong, D. A. *J. Am. Chem. Soc.* **1997**, *119*, 208–217.
- (13) Block, D.; Yu, D.; Armstrong, D.; Rauk, A. *Can. J. Chem.* **1998**, *76*, 1042–1049.
- (14) Jonsson, M.; Wayner, D.; Armstrong, D.; Yu, D.; Rauk, A. *J. Chem. Soc., Perkin Trans. 2* **1998**, *1998*, 1967–1972.
- (15) Rauk, A.; Yu, D.; Armstrong, D. A. *J. Am. Chem. Soc.* **1998**, *120*, 8848–8855.
- (16) Croft, A. K.; Easton, C. J.; Radom, L. *J. Am. Chem. Soc.* **2003**, *125*, 4119–4124.
- (17) Wood, G. P. F.; Moran, D.; Jacob, R.; Radom, L. *J. Phys. Chem. A* **2005**, *109*, 6318–6325.
- (18) Farber, J. M.; Levine, R. L. *J. Biol. Chem.* **1986**, *261*, 4574–4578.
- (19) Stadtman, E.; Oliver, C. *J. Biol. Chem.* **1991**, *266*, 2005–2008.
- (20) Lu, H.-F.; Li, F.-Y.; Lin, S. H. *J. Comput. Chem.* **2007**, *28*, 783–794.
- (21) Cheng, W.-C.; Jang, S.; Wu, C.-C.; Lin, R.-J.; Lu, H.-F.; Li, F.-Y. *J. Comput. Chem.* **2009**, *30*, 407–414.
- (22) Stadtman, E. R. *Annu. Rev. Biochem.* **1993**, *62*, 797–821.
- (23) Kochi, J. K. *J. Am. Chem. Soc.* **1962**, *84*, 1193–1197.
- (24) Galano, A.; Alvarez-Idaboy, J. R.; Cruz-Torres, A.; Ruiz-Santoyo, M. E. *Int. J. Chem. Kinet.* **2003**, *35*, 212–221.
- (25) Galano, A.; Alvarez-Idaboy, J. R.; Cruz-Torres, A.; Ruiz-Santoyo, M. E. *J. Mol. Struct. (THEOCHEM)* **2003**, *629*, 165–174.
- (26) Galano, A.; Alvarez-Idaboy, J. R.; Agacino-Valdés, E.; Ruiz-Santoyo, M. E. *J. Mol. Struct. (THEOCHEM)* **2004**, *676*, 97–103.
- (27) Galano, A.; Alvarez-Idaboy, J. R.; Bravo-Pérez, G.; Ruiz-Santoyo, M. E. *J. Mol. Struct. (THEOCHEM)* **2002**, *617*, 77–86.
- (28) Galano, A.; Alvarez-Idaboy, J. R.; Montero, L. A.; Vivier-Bunge, A. *J. Comput. Chem.* **2001**, *22*, 1138–1153.
- (29) Stefanic, I.; Bonifačić, M.; Asmus, K.-D.; Armstrong, D. A. *J. Phys. Chem. A* **2001**, *105*, 8681–8690.
- (30) Lin, R.-J.; Jang, S.; Wu, C.-C.; Liu, Y.-L.; Li, F.-Y. *J. Comput. Chem.* **2011**, *32*, 3409–3422.
- (31) Honda, S.; Yamasaki, K.; Sawada, Y.; Morii, H. *Structure* **2004**, *12*, 1507–1518.
- (32) Fedorov, D. G.; Ishida, T.; Uebayasi, M.; Kitaura, K. *J. Phys. Chem. A* **2007**, *111*, 2722–2732.
- (33) Kitaura, K.; Ikeo, E.; Asada, T.; Nakano, T.; Uebayasi, M. *Chem. Phys. Lett.* **1999**, *313*, 701–706.
- (34) Barone, V.; Cossi, M. *J. Phys. Chem. A* **1998**, *102*, 1995–2001.
- (35) Cossi, M.; Rega, N.; Scalmani, G.; Barone, V. *J. Comput. Chem.* **2003**, *24*, 669–681.
- (36) Wood, G. P. F.; Gordon, M. S.; Radom, L.; Smith, D. M. *J. Chem. Theory Comput.* **2008**, *4*, 1788–1794.
- (37) Ding, Y.; Krogh-Jespersen, K. *J. Comput. Chem.* **1996**, *17*, 338–349.
- (38) Tortonda, F. R.; Pascual-Ahuir, J. L.; Silla, E.; Tuñón, I. *Chem. Phys. Lett.* **1996**, *260*, 21–26.
- (39) Fernandez-Ramos, A.; Smedarchina, Z.; Siebrand, W.; Zgierski, M. Z. *J. Chem. Phys.* **2000**, *113*, 9714–9721.
- (40) Leung, K.; Rempe, S. B. *J. Chem. Phys.* **2005**, *122*, 184506–184512.
- (41) Balta, B.; Aviyente, V. *J. Comput. Chem.* **2003**, *24*, 1789–1802.
- (42) Amadei, A.; Linssen, A. B. M.; Berendsen, H. J. C. *Proteins: Struct., Funct., Bioinf.* **1993**, *17*, 412–425.
- (43) García, A. E.; Sanbonmatsu, K. Y. *Proteins: Struct., Funct., Bioinf.* **2001**, *42*, 345–354.
- (44) Zhou, R.; Berne, B. J.; Germain, R. *Proc. Natl. Acad. Sci. U.S.A.* **2001**, *98*, 14931–14936.
- (45) Kamiya, N.; Higo, J.; Nakamura, H. *Protein Sci.* **2002**, *11*, 2297–2307.
- (46) Hess, B.; Kutzner, C.; van der Spoel, D.; Lindahl, E. *J. Chem. Theory Comput.* **2008**, *4*, 435–447.
- (47) Frisch, M. J.; Trucks, G. W.; Schlegel, H. B.; Scuseria, G. E.; Robb, M. A.; Cheeseman, J. R.; Montgomery, J. A.; Vreven, T.; Kudin, K. N.; Burant, J. C.; et al. *Gaussian 03*; Gaussian, Inc.: Wallingford CT, 2004.
- (48) Truhlar, D. G.; Gordon, M. S. *Science* **1990**, *249*, 491–498.
- (49) Truhlar, D. G.; Steckler, R.; Gordon, M. S. *Chem. Rev.* **1987**, *87*, 217–236.
- (50) Fukui, K. *J. Phys. Chem.* **1970**, *74*, 4161–4163.
- (51) Garrison, W. M. *Chem. Rev.* **1987**, *87*, 381–398.
- (52) Armstrong, D. A.; Yu, D.; Rauk, A. *Can. J. Chem.* **1996**, *74*, 1192–1199.
- (53) Steinfeld, J. I. F., J.S., Hase, W. L. *Chemical Kinetics and Dynamics*; Prentice-Hall: Upper Saddle River, NJ, 1989.
- (54) Daura, X.; Gademann, K.; Jaun, B.; Seebach, D.; van Gunsteren, W. F.; Mark, A. E. *Angew. Chem., Int. Ed.* **1999**, *38*, 236–240.
- (55) Hansmann, U. H. E. *Chem. Phys. Lett.* **1997**, *281*, 140–150.
- (56) Sugita, Y.; Okamoto, Y. *Chem. Phys. Lett.* **1999**, *314*, 141–151.
- (57) Case, D. A.; Darden, T. A.; Cheatham, T. E., I. I. I.; Simmerling, C. L.; Wang, J.; Duke, R. E.; Luo, R.; Crowley, M.; alker, R. C.; Zhang, W.; et al. *AMBER 10*; University of California: San Francisco, CA, 2008.
- (58) Skodje, R. T.; Truhlar, D. G.; Garrett, B. C. *J. Phys. Chem.* **1981**, *85*, 3019–3023.
- (59) Wang, J.; Wang, W.; Kollman, P. A.; Case, D. A. *J. Mol. Graphics Modell.* **2006**, *25*, 247–260.
- (60) Bayly, C. I.; Cieplak, P.; Cornell, W.; Kollman, P. A. *J. Phys. Chem.* **1993**, *97*, 10269–10280.
- (61) Dunitz, J. D. *Science* **1994**, *264*, 670.